cAMP binding to closed pacemaker ion channels is cooperative

Stefan Kuschke, Susanne Thon, Tina Schwabe, Klaus Benndorf, Ralf Schmauder

Institute of Physiology II, Jena University Hospital, Friedrich Schiller University Jena, 07743 Jena, Germany.

Correspondence to: ralf.schmauder@med.uni-jena.de or klaus.benndorf@med.uni-jena.de

Abstract

Activation of tetrameric hyperpolarization activated cyclic nucleotide-modulated (HCN) ion channels by the binding of cyclic nucleotides is a complex cooperative process. Here we address the cooperativity in the binding process of resting murine mHCN2 channels at the single-molecule level by monitoring the binding of fluorescently labeled cAMP to the four binding sites. The channels were tagged with the fluorescent protein eGFP and were expressed in native cell membranes. We show that the ligand binding to resting mHCN2 channels is positively cooperative. A model-based analysis revealed that ligand binding promotes a transition to a flip state and that both ligand affinity and flip state population increase with the degree of occupation of the binding sites. We conclude that in mHCN2 channels embedded in natural cell membranes subunit cooperativity is not only associated with channel activation but appears already in closed channels if more than one ligand is bound.

Introduction

Hyperpolarization-activated cyclic nucleotide-modulated (HCN) channels[1,2] generate electric rhythmicity in specialized brain neurons and cardiomyocytes[3]. Structurally, these channels are tetrameric nonspecific cation channels and they belong to the superfamily of six-transmembrane domain voltage-gated channels[4-6]. The obligatory activation stimulus of these channels is a sufficiently negative membrane voltage. In addition, the binding of the second messenger cAMP to the four available intracellular cyclic nucleotide-binding domains (CNBDs), one in each subunit, boosters activation by both shifting activation to less negative voltages and accelerating the activation speed[7].

The concentration-activation relationship of HCN2 channels with cAMP can be approximated by a Hill function with Hill coefficients exceeding unity[8]. The fact that these values exceed unity indicates a cooperative effect of cAMP binding on activation. Combined current and binding measurements in ensembles of channels by confocal patch-clamp fluorometry (cPCF)[9] suggested a more intricate type of cooperativity with the sequence positive-negative-positive[10,11]. It is presently unclear how this cooperativity of the subunits emerges, either by events preceding channel activation or by channel activation itself, possibly due to a reciprocal feedback to ligand binding[8], or by both mechanisms. Previous cPCF measurements of the binding kinetics in ensembles of HCN2 channels not activated by voltage showed that description of the ligand binding required a Hill coefficient of 1.28[12]. This result immediately suggests relevant cooperativity among the subunits when cAMP binds, thus ruling out independent cAMP binding to the four subunits also in non-activated channels.

In contrast to these results, a recent single-molecule study on cAMP binding reported that cAMP binds independently to all four subunits in both closed HCN1 and HCN2 channels[13]. The authors performed single-molecule binding measurements with a fluorescent cAMP derivative to isolated receptors positioned in zero-mode waveguides (ZMW). The receptors were purified from HEK293Tcells and solubilized into detergent micelles. These experiments suggested independent cAMP binding and the existence of a flip state following the binding[12]. Together, these data favor a scenario that only hyperpolarization-induced channel activation evokes relevant cooperative interaction of the subunits whereas cAMP binding to the tetrameric CNBD of non-activated channels is independent, leaving, however, the Hill coefficient of 1.28 in macroscopic binding experiments[12] unexplained.

Single molecule detection has become a powerful technique to elucidate details of molecular processes[14,15] at equilibrium. However, most of single-molecule experiments do not directly follow ligand-receptor interaction, though it is the initiating step of most signaling cascades. In some studies ligands were used for continuous reversible labeling in super-resolution microscopy[16] or for label

exchange to compensate for photobleaching, a phenomenon that often limits single-molecule tracking experiments[17,18].

The rareness of studies on ligand binding itself is due to the inherent difficulty of distinguishing between labeled ligands bound to a receptor from free labeled ligands in solution generating unwanted experimental background signal. Several strategies were employed to increase the signal to noise ratio of such experiments: (1) Reduction of the required concentration for binding events by selecting high affinity systems by using mutations to increase the affinity or by using either natural[19,20] or engineered[21,22] ligands with higher affinities. (2) Reduction of the detection volume either mechanically[23] or optically, e.g. with total internal reflection Microscopy (TIRFM)[24] or confocal techniques as fluorescence correlation spectroscopy (FCS)[25,26]. A particular case are zero-mode wave-guides, combining optical and mechanical approaches[27] that were successfully used to investigate ligand binding on isolated binding sites[28,29] or solubilized channels[13]. To the best of our knowledge, only proof of concept experiments with native membranes were reported in planar waveguides[30]. (3) Utilization of brighter fluorophores to reduce relative contributions of the Poisson noise[31].

Here we use a combination of these strategies to enable single-molecule binding measurements: We use a ligand with both increased affinity and brightness compared to previous studies[12,13] and combine these improved properties with TIRF-microscopy to reduce the background fluorescence of free ligands in solution. With these optimizations we investigated the binding of single cAMP molecules to individual native mHCN2 channels embedded in a native molecular environment of the cell membrane and we address the question whether or not under those conditions the stochastic cAMP binding is independent or not. In contrast to the study of White and coworkers[13] we demonstrate cooperativity in ligand binding and we demonstrate that the consecutive binding steps increase both the ligand affinity of the binding sites and the population of a flip state.

Results

While the environment of a native membrane excludes the risk of potential artefacts from channel isolation and reconstitution, additional care needs to be taken to avoid artefacts from the complexity of the native environment. We focused on two aspects: We checked whether our assumptions of immobile channels on the time and length scale of our analysis are valid (Extended Data Fig. 2) and we employed a strategy of completive suppression of spurious nonspecific binding to endogenous cAMP binding proteins (Extended Data: Suppression of f1cAMP binding to endogenous membrane proteins). These experiments helped us to ensure that the observed binding events report binding to eGFPmHCN2 channels and not to other endogenous membrane proteins with cAMP binding sites.

The mobility of eGFPmHCN2 channels in supported native cell membranes is negligible

We investigated the mobility of eGFPmHCN2 channels by selecting a set of positions with a point-spread function (PSF) like signals in both the GFP and ligand signal in the initial images and, subsequently, by tracking the eGFP signal. For this, a 2D Gaussian was fitted to a 7 × 7 pixel area centered with respect to the previous localization coordinates. From the fit coordinates, trajectories were plotted (Extended Data Fig. 2a) and a squared displacement as function of time was calculated (Extended Data Fig. 2c). The latter converged rapidly to a maxima value, likely representing the special resolution at the given signal to noise. This interpretation was confirmed by a trajectory where the observed squared displacement increased after some time. More detailed analysis showed that the increase coincided with GFP photobleaching, e.g. a decrease in the signal to noise ratio. Interestingly, the signal traces from the initial position showed systematically a more stable

signal than traces constructed from the fitted position (Extended Data Fig. 2b), confirming further that the fluctuation in the position is due to a deteriorating fit quality and not due to an increased molecular mobility. In short, no indication of eGFPmHCN2 mobility on the considered length scale was observed. We saw no evidence arguing against the assumption of immobile receptors, which allowed us to use a small (3 × 3) ROI at a fixed position to follow ligand binding to eGFPmHCN2 channels.

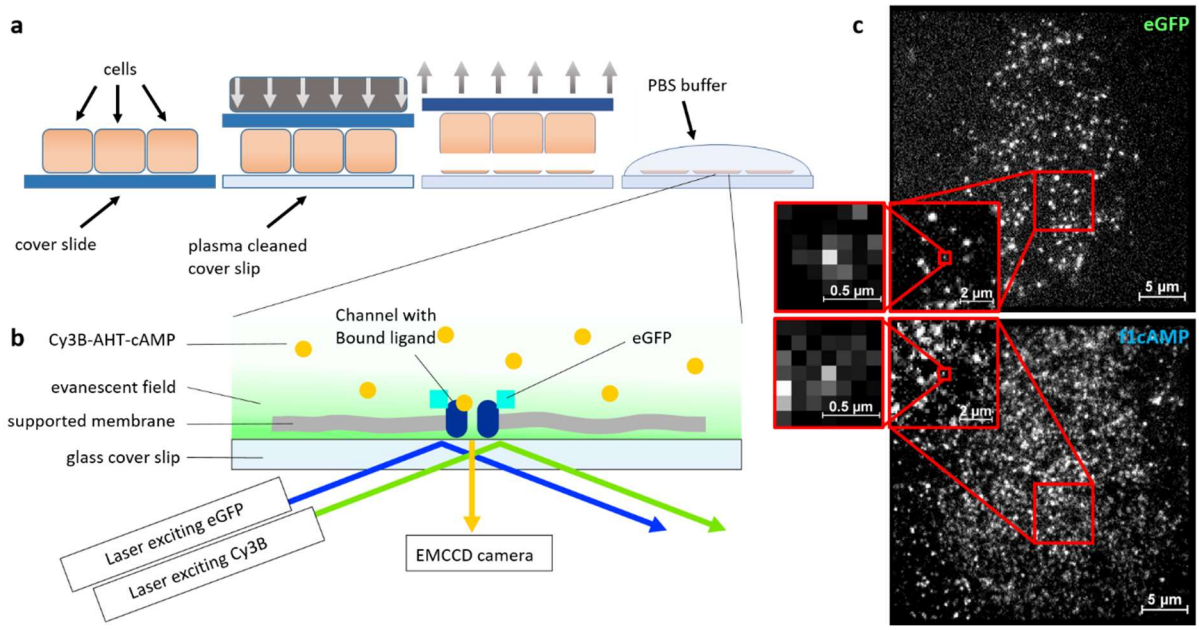

Fig. 1. Generation of supported membrane sheets. a, Supported membrane sheets were generated by using cultured HEK293 cells stably transfected with eGFPmHCN2 and sticking the membrane to cover slips. Cover slips were put upside down onto plasma-cleaned cover slides and pushed down by 5.3 kPa . Cover slips were then removed, leaving the top membrane on the cover slide while the intracellular part was accessible for solutions. **B,** TIRF measurements of fluorescent cAMP derivatives and eGFP tags attached to HCN2 channels were performed on supported membranes. Only ligands near the membrane are excited due to the typical steep exponential decay of the laser power in the evanescent field. **c,** eGFP (top) and f1cAMP (bottom) TIRF recordings of a supported membrane. Individual signals were fitted to a 2D Gaussian function to ensure evaluation of single molecules.

A combination of competitive inhibitors reduces f1cAMP binding to endogenous membrane proteins

We added a mixture of competitive inhibitors for cAMP-binding membrane proteins to suppress binding of f1cAMP (Extended Data Fig. 5). Based on expression data[32] we focused on suppressing binding to protein kinases A (PKA), phosphodiesterases (PDE) and Exchange Protein activated by cAMP (EPAC) by adding Piclamilast[33], 8-pCPT-2-OMe-cAMP[34] and ht31[35], respectively, at relevant concentrations (Extended Data Fig. 5b). The potency of our inhibitor mixture was assessed by comparison to the competitive suppression properties of saturating amounts of cAMP. The mixture was able to suppress 92% of endogenous cAMP binding (Extended Data Fig. 5c). In patch-clamp experiments we confirmed that the mixture does not affect the cAMP action on mHCN2 channels (Extended Data Fig. 5d). Taken together, both the localization of channels by eGFP and the efficacy of our inhibitor mixture renders the contribution of endogenous binding to a negligible level.

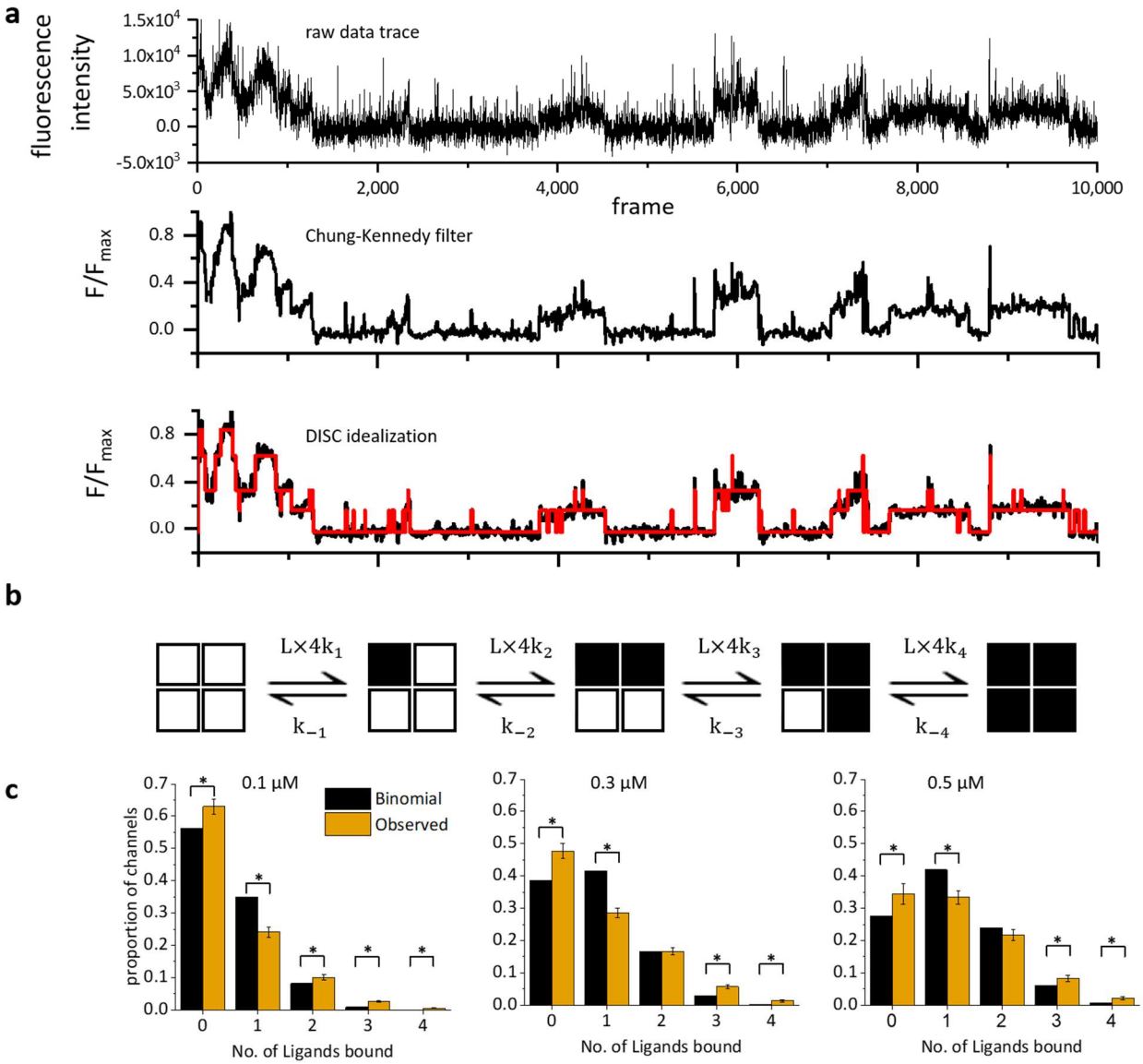

Fig. 2. Recording of binding events and data processing. a, Raw data traces were smoothened by the Chung-Kennedy Filter. Filtered traces were idealized to the number of bound ligands by the DISC algorithm[36]. **b,** Proposed non-cooperative model[13]. Successive binding of ligands does not alter the binding affinity. On- and off-rates differ only in the stochastic availability of binding sites. **c,** The proportion of observed states was compared to the expected proportion of non-cooperative binding calculated by equation (2). Error bars show sem. *indicate significant differences (one sample *t*-test, P<0.05).

f1cAMP binds to HCN2 channels in native membranes in a cooperative manner

To investigate single ligand binding to HCN2 channels embedded in native membranes, we established a stable HEK 293 cell line expressing N-terminally GFP-tagged HCN2 (eGFPmHCN2) using an inducible promoter. The eGFP-HCN2 construct showed voltage activation and ligand modulation comparable to wildtype HCN2 (Extended Data Fig. 1). For visualization of ligand binding, a protocol similar to that of Perez and coworkers[37] was established, yielding native membrane sheets with the intracellular side exposed to solution. Here, specific binding of f1cAMP to the GFP-tagged HCN2 channels was confirmed (Extended Data Fig. 4c). The used f1cAMP allowed us a reliable single-molecule detection at concentrations up to 0.5 µM in TIRFM. Thus, at controlled low expressions (0.2 channels/µm^2), single-ligand binding dynamics to individual HCN2 channels could be followed.

Intensity trajectories for each identified mHCN2 channel were extracted, filtered, and idealized (Fig. 2a). As a model-free approach to detect cooperativity, observed occupancies were compared to the binomially distributed fractions expected for four independent binding sites (Fig. 2b). For each concentration, the number of frames spent in each state of channel ligandation was collected and the fraction of this liganded state with respect to observed states was calculated. For comparison, the expected fraction of each liganded state was calculated according to equations (1) and (2) (see Methods: single molecule analysis). Then, observed and expected fractions were compared for different concentrations (Fig. 2c). At almost each liganded state there is a significant difference between observed and expected proportion of states. The non-liganded state and the highly liganded states with 3 and 4 ligands bound were more abundant in the observation than in the expectation when assuming independent binding. In contrast, the first liganded state was underrepresented as compared to the expected values. For concentrations of 0.3 and 0.5 µM f1cAMP, only the double liganded state matched the expected fractions. This significant deviation from a binomial distribution contradicts independent ligand binding[13]. It should be emphasized, that more complex models of independent binding sites would not alter these equilibrium binding probabilities, because an equal probability of ligand binding independent of the dynamics is assumed in this analysis.

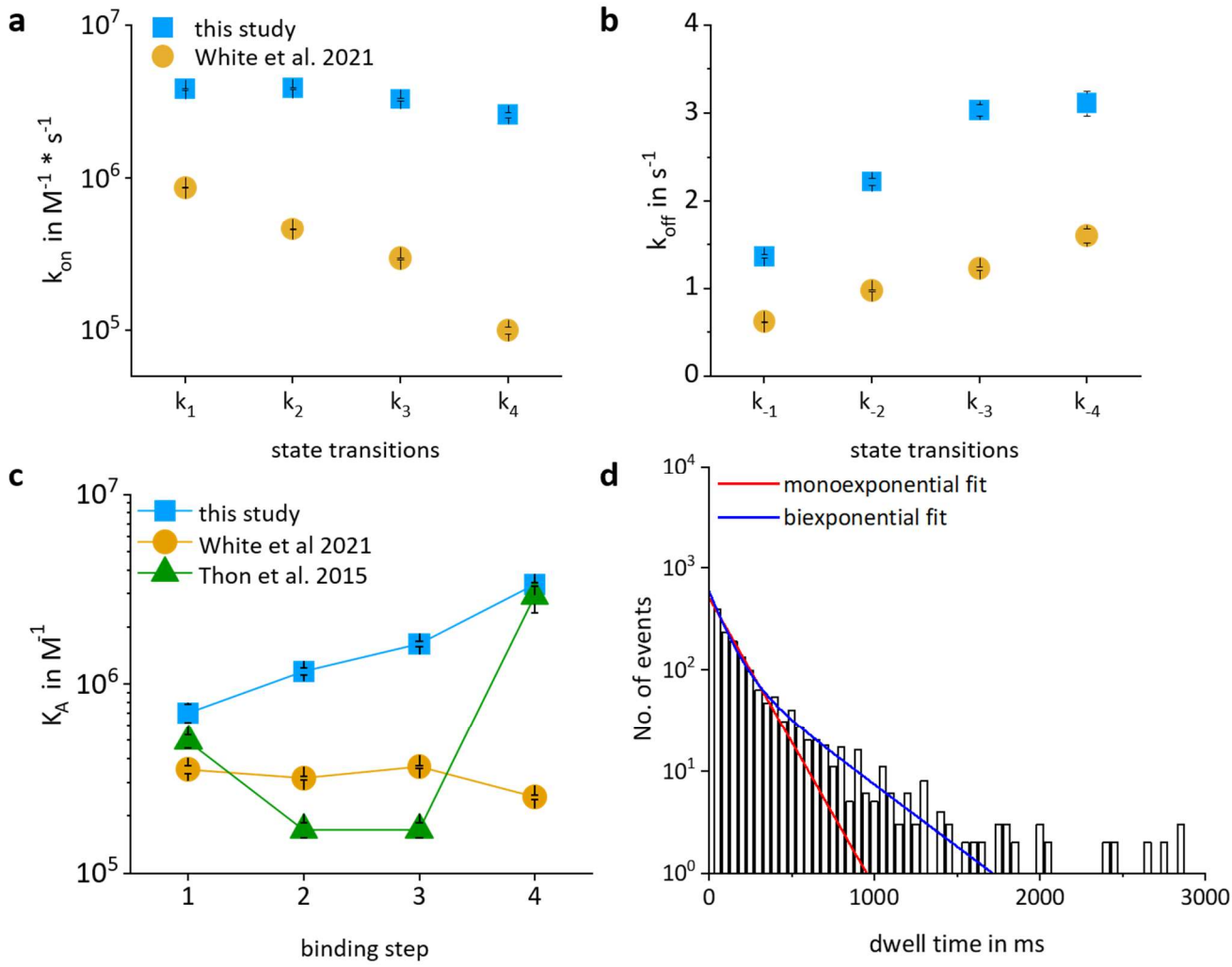

Fig.3. Kinetic and equilibrium constants calculated for a simple binding reaction. a, Comparison of present to previous constants. On-rates of individual binding steps for our data in comparison to on-rates reported by White and coworkers[13]. **b,** Off-rates of individual binding steps. **c,** Association constants of individual binding steps. **d,** Dwell times of isolated single-liganded states at 0.1 µM f1cAMP fitted by a mono- or biexponential function.

To interpret our non-binomial results, we next determined the transition rates for a simple model that includes four consecutive binding steps (Fig. 2b, Extended Data Table 2, model 12) and stoichiometric factors for binding and unbinding. On-rates and off-rates as well as the resulting association constants were calculated (Fig. 3a-c). Binding and unbinding rates were higher than previously reported. Note also that f1cAMP has a higher affinity than the previously used fcAMP[21]. The association constants showed an almost linear increase along the 4 binding steps. This differs from the data shown by White and coworkers[13] where association constants were almost constant throughout the individual binding steps. It also differs from data by Thon and coworkers[12] that showed an initial decrease after the first binding step, followed by a strong increase for the last binding step. These differences could originate from the overly simplistic model-structure.

Ligand binding drives the channels to a flip state

Dwell times of selected single-liganded states that were both preceded and followed by entirely empty states were extracted and analyzed. Histograms were formed and fitted to exponential functions (Fig. 3d). For all concentrations, biexponential fits were required (Extended Data Fig.2). The time constants of the slow component were generally about three times slower than those of the fast component, indicating directly that ligand binding promotes occupation of another state, termed in the following flip state. To further understand the role of such a flip state, we analyzed in total 13 kinetic models (Extended Data Materials, Extended Data Table 2).

Taking both the tetrameric structure with four binding sites and the existence of a flip state into account, we started the modeling with schemes containing 10 states, five resting states and five flip states in a parallel arrangement (model 1 in Extended Data Table 2). In our computations we obeyed the principle of microscopic reversibility[38], saying that in a cycle the product of the rate constants in clockwise direction must equal the product of the rate constants in counter-clockwise direction. This reduces the number of rate constants per cycle by one. The log-likelihood (LL) value was taken as measure for the goodness of the fit and the uncertainty of the parameters is given by the relative SEM (%SEM) of the parameter value (Extended Data Table 3).

Following the strategy described in Extended Data Methods, model 12 turned out to have the most favorite structure (Fig. 4a, Extended Data Table 2). From the rate constants of the individual steps in this model, equilibrium association constants, $K_A=k_x/k_{-x}$, and equilibrium flip constants, $K_F=f_x/f_{-x}$, were calculated. For the resting states, K_A, increases in a non-linear fashion from the first to the fourth binding step (Fig. 4b). In the flip state, the K_A values are larger for the binding steps 2, 3, and 4 with respect to their counterparts in the resting state by about threefold. Similar to the resting state, the association constant stays almost constant for binding step 3 with respect to binding step 2 but almost doubles for binding step 4 with respect to binding step 3. Regarding the flip reaction, the empty and the single-liganded state have about the same K_F value whereas the binding of the ligands 2, 3, and 4 increases K_F strongly in an approximately exponential fashion (Fig. 4c). These results show that also in channels not pre-activated by voltage, the fist binding step is without major effect. In contrast, the second binding step plays a key role for triggering an enhanced ligand binding in the third and fourth binding step. These interpretations by model 12 quantify the pronounced cooperativity of the subunits in the flip reaction following progressive ligand binding.

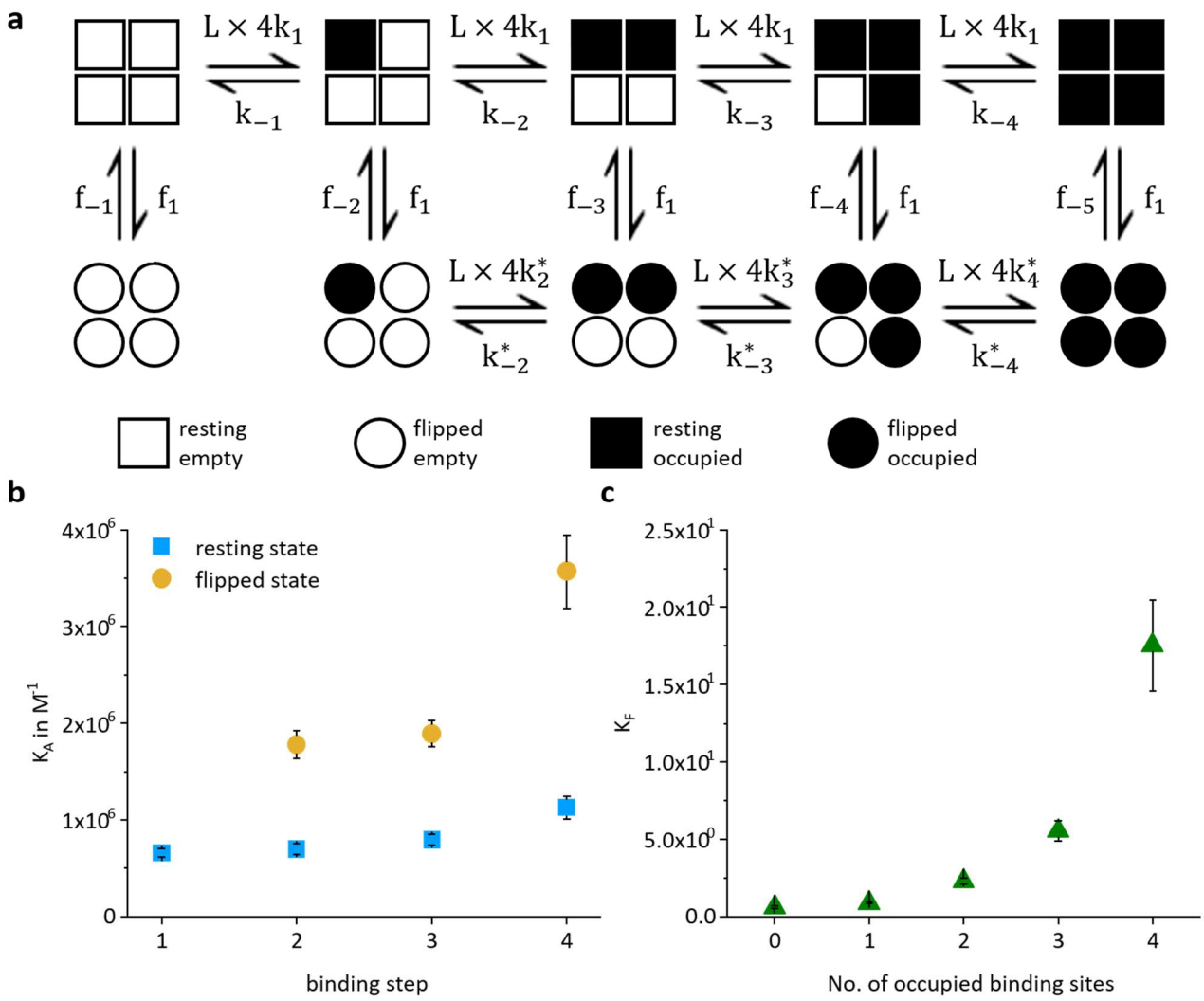

Fig. 4. Favored model to describe the single binding events. a, Scheme of model 13. The model consists of four individual binding steps of which each has an own transition to a flip state. In a flip state, additional binding is possible. Due to extremely small rate constants between the non-liganded and the single-liganded flip state, this transition is excluded. Symbols describe subunit properties. **b,** Equilibrium association constants (K_A) for binding of ligands in the non-flip (blue) and flip state (orange). **c,** Equilibrium constants for switching into the flip state depending on the state of receptor occupation. Error bars show sem.

Discussion

Here we quantified the kinetics of ligand-binding on single resting tetrameric mHCN2 channels that were functionally expressed in native cell membranes using the TIRF microscopy in isolated supported membranes. We demonstrate that the binding process in the resting channels is cooperative and associated with a molecular flip reaction. These results are in contrast to a previous study on single-molecule binding by White and colleagues[13] but are in line with results on previous macroscopic measurements on the kinetics of ligand binding in excised patches[12].

To explain the differences to the results of White and colleagues[13], we consider data collection and analysis in more detail. White and coworkers have published a powerful algorithm to analyze data[36], which we also applied in a modified manner (Extended Data Adaptation of DISC – Algorithm). Our modifications included a minimum difference between identified levels and a comparison to the background, surrounding the identified signal to ensure correct identification of the lowest state

observed. These modifications were tested on simulated data and yielded recovery rates > 95%. They are therefore unlikely to be the source of differences in the results. Additionally, traces were visually checked to avoid falsely identified states (see Extended Data Discussion). Despite these differences, the basically same methodologic approach also provided us evidence for the existence of a relevant flip state in channel activation.

In both single-molecule studies, eGFP-tagged HCN2 channels were used. In contrast, untagged channels were used by Thon and coworkers[12].

In both previous studies the fluorescent cAMP derivative Dy547-aminoethyl-cAMP (fcAMP) was used while we used the superior f1cAMP (Cy3B-AHT-cAMP)[21]. f1cAMP differs from fcAMP in the length of the amino-alkyl linker and the fluorophore. It was shown previously that derivatives containing an aminohexyl-linker have an increased affinity over the derivatives with aminoethyl linkers. Also, Cy3B gives brighter fluorescence than Dy547. Overall, f1cAMP shows an about 2.5 times higher affinity for HCN2 channels than fcAMP[21]. With the lower concentration needed with f1cAMP, we could use conventional TIRF-microscopy with lower disturbing background effects from free ligands in solution than in the study by White and coworkers working with zero-mode wave guides. Additionally, the higher brightness enables faster data acquisition.

Another major difference lies in the sample preparation and, following this, the molecular environment of the channels. While White and coworkers[13] solubilized and purified the channels, and with this put them into an artificial detergent micelle, we studied the binding in native cell membranes. While micelles contain only one protein, in this case the mHCN2 channel, our native membrane contains other proteins potentially binding f1cAMP and thus generating background binding events. To minimize these possible erroneous binding events, we employed two strategies: (I) We utilized eGFP tagged channels and only evaluated binding signals with point-spread-function (PSF) like shapes that where closely colocalized to the PSF-shaped eGFP signal. (II) We reduced the influence of endogenous binding sites by adding a mixture of selective competitive inhibitors and washing binding sites off (Extended Data Methods). The functionality of our mHCN2 channels was not altered by these inhibitors for other binding sites as shown by patch-clamp recordings (Extended Data Fig. 4). Taken together, we suggest that the functional difference between our results and those of White and coworkers – cooperativity versus non-cooperativity in ligand binding – are the consequence of the different nature of the membranes surrounding the channel.

Relevant influences of the membrane composition of micelles on either the structure or function of membrane proteins is a well-known phenomenon. For example, Cao and coworkers[39] showed for mGlu2 receptors that the interaction between membrane forming lipids and the receptor is required for function. Protein function was preserved best when a mixture of cholesterol hemi succinate (CHS), glyco-diosgenin (GDN) and lauryl maltose neopentyl glycol was used for micelle formation. With regard to HCN channels, a direct context between membrane composition and channel function was reported by Fürst and D'Avanzo[40] who investigated the role of cholesterol on activation kinetics, deactivation kinetics and current density in cells. While for HCN1 there was no significant effect on activation or deactivation kinetics at cholesterol enrichment or depletion, the deactivation kinetics of HCN2 slowed down upon cholesterol enrichment. Though Fürst and D'Avanzo[40] did not consider cooperativity phenomena, their results with cholesterol enriched membranes might result from cooperativity changes. Interestingly, White and coworkers[13] had to optimize the detergent condition to obtain stable sample preparations for different HCN-Isoforms. For HCN1, their detergents included CHS, a cholesterol mimetic, for purification of proteins. For HCN2, this was substituted to digitonin and the micelles were formed from GDN alone, which also has a cholesterol-related structure.

To quantify the mode of cooperativity we fitted a series of kinetic models and subsequently adopted the following three assumptions: (1) Binding rates to resting channel subunits were set to be equal after accounting for microscopic stoichiometry. (2) Rates of entering the flip state were linked to increase the accuracy of the determined parameters while off-rates were kept independent to account for possible ligand protein interactions stabilizing the flip state. (3) Binding to neighboring subunits was not distinguished from that to opposite subunits and among the neighboring subunits also not between the right and the left neighbor. We assume this is justified as no respective difference was reported for channel activation in mutated concatamers[41]. With these assumptions the best model was chosen based on the certainty of the estimated parameters and the LL. Binding rates did not exceed diffusion limited binding[42]. In fact they were comparable to values published for related isolated binding sites[41]. Altogether, our modelling suggests for resting mHCN2-channels (I) cooperativity in ligand binding, (II) a transition to a flip state that is favored with increased occupation of the binding sites, and (III) that ligand binding is possible in both resting and flipped channels. In our considerations, the flip transition is assigned to the whole channel, as in most classical cooperative models including the Monod-Wyman-Changeux model[43].

While standing in contrast to data from White and coworkers[13] concerning cooperativity, our study agrees with data reported by Thon et al.[12] in which the ligand binding to non-activated HCN2 channels were determined in a macroscopic approach. Affinities of individual binding steps were shown to be cooperative, even if the mode of cooperativity observed here differs from these findings. A flip state was hypothesized by both groups. The models derived here and in Thon and coworkers differ mainly by the flip states not being able to bind additional ligands and the limitation that the association rates of the second and third binding step are set equal. While their recordings were also done in a natural membrane surrounding, the expression system differed - *Xenopus laevis* oocytes there and HEK293 cells here. The type of cooperativity, however, was different in both studies. In our experiments the affinity increases with each binding step whereas Thon et al.[12] determined first a decrease of affinity that is followed by an increase of affinity in subsequent ligand binding. Whether this difference is due to the different sensitivity of single-molecule equilibrium approaches and macroscopic concentration-jumps, to limits in the evaluated models, to variation in the properties of the slightly different fluorescent ligands, or to the different expression systems is not clear.

In conclusion, our data demonstrate that the subunits in resting HCN2 channels act in a cooperative fashion when ligands bind to the four binding sites and that this cooperative action of the subunits is associated with the transition to a flip state.

Material and Methods

Chemicals

Chemicals were purchased and used with no further purification: 8-pCPT-2'OMe-cAMP (Biolog LSI GmbH & Co KG, Bremen, Germany), Trolox, Piclamilast, Glucose oxidase, Catalase, Glucose, Poly-L-Lysin (Merck KGaA, Darmstadt, Germany), ht31 was synthesized on demand (Genosphere Biotechnologies, Clamart, France), Cy3B-AHT-cAMP was synthesized in house as described previously[21].

Cell Culture

HEK293 cell lines containing an inducible promoter (Flp-In-T-REx 293; Invitrogen #R78007) were cultured in minimum essential medium (MEM, (Thermo Fisher Scientific, Schwerte, Germany)) supplemented with 10% fetal calf serum (BioWest, Nuaillé, France), non-essential amino acids (Gibco) and antibiotics according to the manufacturer's instructions. For stable cell lines, Flp-In-T-REx 293 cells were transfected using the calcium phosphate method with a mixture of plasmids (0.5 µg eGFPmHCN2 and 1.5 µg pOG44). After hygromycin B treatment, stable clones were selected and cultured until a passage number of approximately 20. eGFPmHCN2 contains an eGFP linked by a 6-amino acids linker (SDPNST) to mHCN2 (NM_008226)[44].

For single molecule measurements, cells were plated on cover slips (13 mm diameter, #1 - 0.15 mm thickness, Menzel Gläser, Braunschweig, Germany) in 24 well plates. Cover slips were coated with poly-L-lysin before use (0.1 mg/mL poly-L-lysine solution for 2 h followed by multiple washes with media). Per cover slip, 200 µL of resuspended cells (500 cells/µL) culture were added. Cells were allowed to settle a day before induction of protein expression with media supplemented with 0.2 µg/mL tetracycline (Sigma-Aldrich, Taufkirchen, Germany). Cells were used 2 to 48 h after induction.

Membrane preparation

Cells grown on cover slips were washed three times with sterile filtered PBS (300 µL). Cover slides (25 mm diameter, #1 - 0.15 mm thickness, Menzel Gläser, Braunschweig, Germany), prior to usage cleaned by Zepto Plasma cleaner (Diener Electronics, Ebhausen, Germany), were mounted in Attofluor imaging chambers (Thermo Fisher Scientific, Schwerte, Germany). Cover slips were inverted onto plasma cleaned cover slides with 20 µL PBS in-between the glasses. Additional weight (0.7 N) was put onto the glass slips for 5 minutes. After taking off the weight, the upper glass slip was removed using an EDSYN LP200 Pixter Pen-Vac pneumatice forceps (EDSYN Inc., Van Nuys, USA) leaving supported membrane attached to the lower, plasma cleaned cover slide. The cover slide with the attached membrane was washed three additional times with sterile filtered PBS. A solution of 100 µM ht31 in sterile filtered PBS was added and replaced after 5 minutes with sterile filtered PBS. Afterwards, membranes were incubated with a solution of f1cAMP (Cy3B-AHT-cAMP)[21,45], a competitive inhibitor for membrane associated cAMP binding proteins (8-pCPT-2'OMe-cAMP, Piclamilast), an oxygen scavenger system (165 U/mL Glucose oxidase, 2170 U/mL Catalase, 0.4 w% Glucose) and 2 mM Trolox. The system was allowed to equilibrate for 5 minutes before imaging.

Single Molecule Microscopy

Membranes were positioned first in the widefield of a microscope and then investigated by TIRFM. Measurements were performed on a Nikon Eclipse Ti inverse microscope using an Apochromat 1.49/100 x oil objective (Nikon Europe B.V., Amstelveen, Netherlands) together with Immersol™ 518F (Zeiss, Jena, Germany). Data was recorded by an Andor iXon 888 Ultra camera (Oxford Instruments, Tubney Woods, Abingdon, United Kingdom) equipped with an LS-OC optomask (Cairn

Research Ltd, Faversham, United Kingdom) controlled with NIS-Elements AR 5.02.02. Single-molecule recordings were performed in a 256 x 256 pixel ROI in the camera's isolated cop mode. Movies of 10,000 frames (exposure time 10 ms, ≈88 fps, 115 s) of the cAMP signal were followed by movies of 3,000 frames (exposure time 40 ms; ≈25 fps; 75 s) of the eGFP s signal. Excitation and emission were filtered using appropriate filter sets (AHF Analysentechnik AG, Tübingen, Germany): eGFP-excitation: 472/30 Brighline HC, dichroic: zt 488 RDC, emission: 515/30 BrightLine HC (Semrock); f1cAMP: dichroic: ZT543rdc, emission: 596/83 BrightLine HC.

In widefield, eGFP was excited with a dimmed Nikon Intensilight lamp. For single molecule recording, eGFP was excited by a Stradus® 488-150 VORTRAN Laser (LASER TECHNOLOGY, INC, City, USA/ Frankfurt Laser Company, Friedrichsdorf, Germany). Fluorescent f1cAMP derivatives were excited by a 100 mW MLL-III-543/1~100 mW laser (Changchun New Industries Optoelectronics Tech. Co., Changchun, China). Lasers were controlled by an AOTF included in the Nikon Laser Box LU4A.

Single molecule analysis

Time trajectories of single molecules binding and unbinding were extracted using MATLAB 2020b (Mathworks). Positions of binding and unbinding events were matched to positions of eGFP bleaching signals to select the positions of mHCN2 channels. Each frame contained 256 x 256 pixels of 0.13 µm x 0.13 µm in size in the object plane. Background signals were removed by subtracting a median filtered movie (median Kernel: 9 x 9 x 3).

Single molecules were identified by iteratively selecting subsequent signal maxima in a maximal intensity projection of the background-subtracted movie and fitting a 2D Gaussian to 5 × 5 pixel around the maxima. Positions with fit results showing half axes wider than 2 pixels were rejected. The process was repeated at the same location for the eGFP-Signal. Due to the worse signal-to-noise ratio in the eGFP signal, leading to poorer fits, fits with half axes exceeding 3.3 pixels were rejected. If both the f1cAMP signal and the eGFP signal were present at the same position, the data trace was used for further analysis. The sum of a 3 x 3 area around the original location was used as signal for the traces. Traces were filtered by Chung-Kennedy filter with p, N and M being 40, [4 8 16 32] and 10[46]. This signal still contained sparse and unusually bright one or two frame events, which were removed by a 5-point median filter.

Traces of f1cAMP and eGFP signals were inspected by eye and included if they showed stepwise changes in average intensity. Traces were then idealized using a modified version of the DISC algorithm[36] . Modifications included a minimum threshold between individual intensities and a correction for traces that never reached a state in which no ligands are bound during a measurement (extended data Adaptation of DISC – Algorithm). All idealized traces were inspected by eye following idealization. Accepted traces accumulated to 1.6 x 10^4 s of measurements across approximately 150 mHCN2 channels at f1cAMP concentrations of 0.1, 0.3 and 0.5 µM. Statistical analysis was performed using MATLAB 2020b unless otherwise stated.

From observed states the average probability of a ligand binding to a subunit, *P*(1), was calculated using

$$P(1) = \frac{N(1) + 2 * N(2) + 3 * N(3) + 4 * N(4)}{4 * (N(0) + N(1) + N(2) + N(3) + N(4))} \quad (1)$$

With N(x) being the number of frames spent in with x ligands bound. P(1) was used to calculate expected binomial distribution according to:

$$F(x) = \binom{4}{x} P(1)^x * \left(1 - P(1)\right)^{4-x} \quad (2)$$

With F(x) being the expected fraction of x Ligands bound.

Dwell times of single-liganded channels that were preceded and followed by states in which no ligand was bound, were extracted and binned in a histogram. Mono- and biexponential distributions were fitted to the data. Functions follow the form of $Y = A_1 * e^{-\frac{x}{\tau_1}}$ (monoexponential) and $Y = A_1 * e^{-\frac{x}{\tau_1}} + A_2 * e^{-\frac{x}{\tau_2}}$ (biexponential).

Modeling

Models differing in the combination of independent or equated rate constants were created. Additionally, it was considered whether the flip state can bind ligands. The rate constants of these models were determined by the QuB software[47]. First and last state transitions were excluded before analysis. Models were optimized globally over a set of three f1cAMP concentrations ranging from 0.1 to 0.5 µM using maximum idealized point optimization[48]. The quality of optimization was evaluated by ranking the maximum likelihood.

Literature

1 Ludwig, A., Zong, X., Jeglitsch, M., Hofmann, F. & Biel, M. A family of hyperpolarization-activated mammalian cation channels. *Nature* **393**, 587-591 (1998).

2 Ludwig, A. *et al.* Two pacemaker channels from human heart with profoundly different activation kinetics. *The EMBO Journal* **18**, 2323-2329 (1999).

3 Biel, M., Wahl-Schott, C., Michalakis, S. & Zong, X. Hyperpolarization-Activated Cation Channels: From Genes to Function. *Physiol Rev* **89**, 847-885, doi:10.1152/physrev.00029.2008.-Hyperpolarization-activated (2009).

4 Li, M. *et al.* Structure of a eukaryotic cyclic-nucleotide-gated channel. *Nature* **542**, 60-65, doi:10.1038/nature20819 (2017).

5 Lee, C. H. & MacKinnon, R. Structures of the Human HCN1 Hyperpolarization-Activated Channel. *Cell* **168**, 111-120.e111, doi:10.1016/j.cell.2016.12.023 (2017).

6 Yu, F. H., Yarov-Yarovoy, V., Gutman, G. A. & Catterall, W. A. Overview of molecular relationships in the voltage-gated ion channel superfamily. *Pharmacological Reviews* **57**, 387-395, doi:10.1124/pr.57.4.13 (2005).

7 Wang, J., Chen, S., Nolan, M. F. & Siegelbaum, S. A. Activity-Dependent Regulation of HCN Pacemaker Channels by Cyclic AMP: Signaling through Dynamic Allosteric Coupling. *Neuron* **36**, 451-461 (2002).

8 Kusch, J. *et al.* Interdependence of receptor activation and ligand binding in hcn2 pacemaker channels. *Neuron* **67**, 75-85, doi:10.1016/j.neuron.2010.05.022 (2010).

9 Biskup, C. *et al.* Relating ligand binding to activation gating in CNGA2 channels. *Nature* **446**, 440-443, doi:10.1038/nature05596 (2007).

10 Benndorf, K., Thon, S. & Schulz, E. Unraveling subunit cooperativity in homotetrameric HCN2 channels. *Biophysical Journal* **103**, 1860-1869, doi:10.1016/j.bpj.2012.09.024 (2012).

11 Kusch, J. *et al.* How subunits cooperate in cAMP-induced activation of homotetrameric HCN2 channels. *Nature Chemical Biology* **8**, 162-169, doi:10.1038/nchembio.747 (2012).

12 Thon, S., Schulz, E., Kusch, J. & Benndorf, K. Conformational Flip of Nonactivated HCN2 Channel Subunits Evoked by Cyclic Nucleotides. *Biophysical Journal* **109**, 2268-2276, doi:10.1016/j.bpj.2015.08.054 (2015).

13 White, D. S. *et al.* cAMP binding to closed pacemaker ion channels is non-cooperative. *Nature* **595**, 606-610, doi:10.1038/s41586-021-03686-x (2021).

14 Weiss, S. Fluorescence Spectroscopy of Single Biomolecules. *Science* **283**, 1676-1683 (1999).

15 Yang, Z., Xu, H., Wang, J., Chen, W. & Zhao, M. Single-Molecule Fluorescence Techniques for Membrane Protein Dynamics Analysis. *Applied Spectroscopy* **75**, 491-505, doi:10.1177/00037028211009973 (2021).
16 Sousa, A. A. & Kruhlak, M. J. in *Nanoimaging Methods and Protocols* Vol. 950 95-110 (Humana Press, Totowa, NJ, 2012).
17 Guignet, E. G., Segura, J. M., Hovius, R. & Vogel, H. Repetitive reversible labeling of proteins at polyhistidine sequences for single-molecule imaging in live cells. *ChemPhysChem* **8**, 1221-1227, doi:10.1002/cphc.200700065 (2007).
18 Lill, Y. *et al.* Kinetics of the initial steps of G protein-coupled receptor-mediated cellular signaling revealed by single-molecule imaging. *ChemPhysChem* **6**, 1633-1640, doi:10.1002/cphc.200500111 (2005).
19 Grandl, J. *et al.* Fluorescent epibatidine agonists for neuronal and muscle-type nicotinic acetylcholine receptors. *Angewandte Chemie - International Edition* **46**, 3505-3508, doi:10.1002/anie.200604807 (2007).
20 Schmauder, R., Kosanic, D., Hovius, R. & Vogel, H. Correlated optical and electrical single-molecule measurements reveal conformational diffusion from ligand binding to channel gating in the nicotinic acetylcholine receptor. *ChemBioChem* **12**, 2431-2434, doi:10.1002/cbic.201100302 (2011).
21 Otte, M. *et al.* Novel Fluorescent Cyclic Nucleotide Derivatives to Study CNG and HCN Channel Function. *Biophysical Journal* **116**, 2411-2422, doi:10.1016/j.bpj.2019.05.006 (2019).
22 Rosier, N. *et al.* A Versatile Sub-Nanomolar Fluorescent Ligand Enables NanoBRET Binding Studies and Single-Molecule Microscopy at the Histamine H3Receptor. *Journal of Medicinal Chemistry* **64**, 11695-11708, doi:10.1021/acs.jmedchem.1c01089 (2021).
23 Leslie, S. R., Fields, A. P. & Cohen, A. E. Convex lens-induced confinement for imaging single molecules. *Analytical Chemistry* **82**, 6224-6229, doi:10.1021/ac101041s (2010).
24 Laasfeld, T. *et al.* Budded baculoviruses as a receptor display system to quantify ligand binding with TIRF microscopy. *Nanoscale* **13**, 2436-2447, doi:10.1039/d0nr06737g (2021).
25 Wohland, T., Friedrich, K., Hovius, R. & Vogel, H. Study of ligand-receptor interactions by fluorescence correlation spectroscopy with different fluorophores: Evidence that the homopentameric 5- hydroxytryptamine type 3(As) receptor binds only one ligand. *Biochemistry* **38**, 8671-8681, doi:10.1021/bi990366s (1999).
26 Grime, R. L. *et al.* Single molecule binding of a ligand to a G-protein-coupled receptor in real time using fluorescence correlation spectroscopy, rendered possible by nano-encapsulation in styrene maleic acid lipid particles. *Nanoscale* **12**, 11518-11525, doi:10.1039/d0nr01060j (2020).
27 Levene, M. J. *et al.* Zero-Mode Waveguides for Single-Molecule Analysis at High Concentrations. 682-686 (2003).
28 Goldschen-Ohm, M. P., White, D. S., Klenchin, V. A., Chanda, B. & Goldsmith, R. H. Observing Single-Molecule Dynamics at Millimolar Concentrations. *Angewandte Chemie* **56**, 2399-2402, doi:10.1002/ange.201612050 (2017).
29 Goldschen-Ohm, M. P. *et al.* Structure and dynamics underlying elementary ligand binding events in human pacemaking channels. *eLife*, doi:10.7554/eLife.20797.001 (2016).
30 Danelon, C., Perez, J. B., Santschi, C., Brugger, J. & Vogel, H. Cell membranes suspended across nanoaperture arrays. *Langmuir* **22**, 22-25, doi:10.1021/la052387v (2006).
31 Schirripa Spagnolo, C. & Luin, S. Choosing the Probe for Single-Molecule Fluorescence Microscopy. *International Journal of Molecular Sciences* **23**, doi:10.3390/ijms232314949 (2022).
32 Rouillard, A. D. *et al.* The harmonizome: a collection of processed datasets gathered to serve and mine knowledge about genes and proteins. *Database : the journal of biological databases and curation*, 1-16 (2016).
33 Card, G. L. *et al.* Structural basis for the activity of drugs that inhibit phosphodiesterases. *Structure* **12**, 2233-2247, doi:10.1016/j.str.2004.10.004 (2004).

34 Schwede, F. *et al.* Structure-Guided Design of Selective Epac1 and Epac2 Agonists. *PLoS Biology* **13**, doi:10.1371/journal.pbio.1002038 (2015).
35 Herberg, F. W., Maleszka, A., Eide, T., Vossebein, L. & Tasken, K. Analysis of A-kinase anchoring protein (AKAP) interaction with protein kinase a (PKA) regulatory subunits: PKA isoform specificity in AKAP binding. *Journal of Molecular Biology* **298**, 329-339, doi:10.1006/jmbi.2000.3662 (2000).
36 White, D. S., Goldschen-Ohm, M. P., Goldsmith, R. H. & Chanda, B. Top-down machine learning approach for high-throughput single-molecule analysis. *eLife* **9**, doi:10.7554/eLife.53357 (2020).
37 Perez, J. B., Martinez, K. L., Segura, J. M. & Vogel, H. Supported cell-membrane sheets for functional fluorescence imaginig of membrane proteins. *Advanced Functional Materials* **16**, 306-312, doi:10.1002/adfm.200500236 (2006).
38 Cantor, C. R. & Schimmel, P. R. *Biophysical Chemistry: Part III: The Behavior of Biological Macromolecules*. 1 edn, (1980).
39 Cao, A. M. *et al.* Allosteric modulators enhance agonist efficacy by increasing the residence time of a GPCR in the active state. *Nature Communications* **12**, doi:10.1038/s41467-021-25620-5 (2021).
40 Fürst, O. & D'Avanzo, N. Isoform dependent regulation of human HCN channels by cholesterol. *Scientific Reports* **5**, doi:10.1038/srep14270 (2015).
41 Sunkara, M. R., Schwabe, T., Ehrlich, G., Kusch, J. & Benndorf, K. All four subunits of HCN2 channels contribute to the activation gating in an additive but intricate manner. *J Gen Physiol* **150**, 1261-1271, doi:10.1085/jgp.201711935 (2018).
42 Van Holde, K. E. A hypothesis concerning diffusion-limited protein-ligand interactions. *Biophysical Chemistry* **101-102**, 249-254 (2002).
43 Monod, J., Wyman, J. & Changeux, J. P. On the Nature of Allosteric Transitions: A Plausible Model. *J Mol Biol* **12**, 88-118, doi:10.1016/s0022-2836(65)80285-6 (1965).
44 Yüksel, S. *et al.* Uncoupling of Voltage- and Ligand-Induced Activation in HCN2 Channels by Glycine Inserts. *Frontiers in Physiology* **13**, doi:10.3389/fphys.2022.895324 (2022).
45 Pfleger, C. *et al.* Allosteric signaling in C-linker and cyclic nucleotide-binding domain of HCN2 channels. *Biophysical Journal* **120**, 950-963, doi:10.1016/j.bpj.2021.01.017 (2021).
46 Chung, S. H. & Kennedy, R. A. Forward-backward non-linear filtering technique for extracting small biological signals from noise. *Journal of Neuroscience Methods* **40**, 71-86 (1991).
47 Nicolai, C. & Sachs, F. Solving Ion Channel Kinetics with the QuB Software. *Biophysical Reviews and Letters* **08**, 191-211, doi:10.1142/S1793048013300053 (2013).
48 Milescu, L. S., Yildiz, A., Selvin, P. R. & Sachs, F. Maximum likelihood estimation of molecular motor kinetics from staircase dwell-time sequences. *Biophysical Journal* **91**, 1156-1168, doi:10.1529/biophysj.105.079541 (2006).
49 Moller, S. *et al.* Cyclic nucleotide mapping of hyperpolarization-activated cyclic nucleotide-gated (HCN) channels. *ACS Chemical Biology* **9**, 1128-1137, doi:10.1021/cb400904s (2014).
50 Schindler, R. F. R. & Brand, T. The Popeye domain containing protein family - A novel class of cAMP effectors with important functions in multiple tissues. *Progress in Biophysics and Molecular Biology* **120**, 28-36, doi:10.1016/j.pbiomolbio.2016.01.001 (2016).

Author contributions:

K.B. and R.S. envisioned the project, S.T. and R.S. established the single molecule measurement technique, S.K. and S.T. performed the single molecule measurements, T.S. engineered the HEK293 cell line with inducible eGFPmHCN2 channel, S.K. and S.T. performed the patch clamp measurements, S.K. and R.S. wrote custom scripts and analyzed data, S.K., R.S. and K.B. wrote the manuscript

Acknowledgement:

We thank K. Schoknecht, S. Bernhardt and C. Ranke for excellent technical assistance.

Competing interests
The authors declare no competing interests.